Fully-Polarimetric GLRTs for Detecting Scattering Centers with Unknown Amplitude, Phase, and Tilt Angle in Terrain Clutter

Ronald L. Dilsavor

Tactical Systems Division / Dayton
Sverdrup Technology, Inc.
Beavercreek, OH 45431

Randolph L. Moses

Department of Electrical Engineering
The Ohio State University
Columbus, OH 43210

ABSTRACT

We present a family of polarimetric generalized likelihood ratio tests (PGLRTs) which exploit fully-polarimetric information in a high resolution application to detect scattering centers in terrain clutter. The detectors are based on a deterministic target model derived from the Huynen parameterization of a scattering matrix. The model is parameterized by target amplitude, absolute phase, and target orientation angle. These parameters, which are unknown in many practical applications, are estimated by the detectors. The PGLRTs may be used to enhance the responses of certain scattering center types relative to others in a given region of interest. Once a scattering center is detected the ML estimates formed by a PGLRT may be used to further describe the detected target. The single-pixel test that we discuss may be extended to multi-pixel tests which compress distributed target response energy.

We implement and analyze the performance of the PGLRTs designed for Gaussian and K-distributed clutter with known covariance. The PGLRT that assumes all three model parameters are unknown is a detector whose performance we show to lie between that of the Optimal Polarimetric Detector and the Polarization Whitening Filter.

1. INTRODUCTION

There are a variety of polarimetric target detectors available in the literature. Among these are the span detector [1,2], polarization whitening filter (PWF) [3,1,2,4], polarization matched filter (PMF) [1,5], optimal polarimetric detector for Gaussian clutter (OPD) [1,5], and the optimal polarimetric detector for K-distributed clutter (OPDK) [1]. The span and PWF do not explicitly distinguish between target and clutter scattering characteristics. The span detector, PWF, and PMF do not make any assumptions on the clutter distribution and the OPDG is specifically designed for Gaussian clutter. The OPDG and OPDK treat the target statistically, like clutter, resulting in a test that chooses between hypotheses with common means and uncommon covariances.

Our goal is to derive a detector of certain canonical scattering center types in terrain clutter given the fully-polarimetric response at a single image resolution cell or pixel. In doing so, we wish to exploit knowledge of the clutter distribution and partial knowledge of the polarimetric target response. We choose a deterministic target response representation for two main reasons: 1) partial knowledge of the response is more easily incorporated into the representation and 2) we consider a high resolution radar application in which major target scattering centers are resolved. The use of the random target representation is more justified in the case of a low resolution radar in which target scattering centers are not resolved.

We present a deterministic target model that is parameterized by up to three unknown parameters; target amplitude, phase, and orientation angle about the radar line of sight. We design generalized likelihood ratio tests to detect signals with these unknown parameters and we compare their performance with that of existing polarimetric detectors. The PGLRT that assumes all three parameters are unknown is a detector whose performance we find to lie between that of the OPD and PWF.

Several families of distributions have been used to model terrain clutter scattering. Gaussian statistics have been assumed in many instances to classify terrain types and to reduce speckle while enhancing target components [1,6,7].

But experimental evidence has shown that many terrain clutter distributions typically have a shape that is "heavy-tailed" when compared to that of a Gaussian distribution. Product models such as the Weibull, lognormal, and K-distributions have been found to more accurately model these heavy-tail distributions and have been used in target enhancement and clutter suppression techniques [2–11]. Although there does not seem to be a consensus of opinion regarding which models are best for many clutter environments, the K-distribution has been successful at modeling forest clutter [8]. We provide detection results for both Gaussian and K-distributed clutter.

In the next section, we describe the signal models used for target scattering centers and for clutter. In Section 3, we theoretically describe a family of polarimetric GLRTs and relate them to existing polarimetric detectors. In Section 4, we provide theoretical and simulated performance curves for these detectors. Section 5 presents our conclusions.

2. POLARIMETRIC SIGNAL MODEL

It is convenient for the purpose of setting up target detection problems to represent the fully-polarimetric measurements in vector form. We use two such vector representations; the complex 3-vector $\vec{X}_c$ and the real 6-vector $\vec{X}_r$ defined as

$$\vec{X}_c \triangleq [\ X_{hh}\quad \sqrt{2}X_{hv}\quad X_{vv}\ ]^T$$
$$\vec{X}_r \triangleq [\ \Re X_{hh}\quad \Im X_{hh}\quad \sqrt{2}\Re X_{hv}\quad \sqrt{2}\Im X_{hv}\quad \Re X_{vv}\quad \Im X_{vv}\ ]^T. \tag{1}$$

We have assumed that the measurements are made in (or are transformed to) the linear horizontal, linear vertical polarization basis. The scattering coefficient X_{vh} has been omitted from these vectors because of the redundancy $X_{vh} = X_{hv}$ in this application. If X_{vh} is measured, then it can be used to give a better estimate of X_{hv}. The $\sqrt{2}$ factors compensate for omitting X_{vh}.

We consider the binary hypothesis test

$$H_0: \quad \vec{X}_c = \vec{C}_c$$
$$H_1: \quad \vec{X}_c = \vec{C}_c + \vec{T}_c(\vec{\Theta}) \tag{2}$$

where H_0 is the clutter-only hypothesis and H_1 is the clutter+target hypothesis. We can also state the hypothesis test using the real 6-vector representation. Note that H_1 is a composite hypothesis due to the dependence of the target component on an unknown parameter vector $\vec{\Theta}$. The elements of $\vec{\Theta}$ are the scattering center amplitude, absolute phase, and orientation angle about the radar line of sight (out-of-plane rotation). Our approach is to design a generalized likelihood ratio test [12] for detecting target presence by replacing the unknown $\vec{\Theta}$ with its ML estimate and setting up the likelihood ratio test. We next describe our models for the target and clutter components.

2.1 Target Model

In order to derive a parameterized model for the target contribution $\vec{T}_c(\vec{\Theta})$ to the measurement vector $\vec{X}_c$ we begin with some known results that apply to the scattering matrix. Let **S** given by

$$\mathbf{S} = \begin{bmatrix} S_{hh} & S_{hv} \\ S_{vh} & S_{vv} \end{bmatrix}$$

be the complex $(I + jQ)$ scattering matrix at a pixel in a synthetic aperture radar image. The elements of **S** are the scattering coefficients S_{xy} corresponding to transmit polarization y and receive polarization x.

Huynen [13] has expressed a general complex symmetric scattering matrix in terms of several geometrically relevant

descriptors:

$$\mathbf{S} = ae^{j\rho}\mathbf{U}^*(\psi,\tau,\nu) \begin{bmatrix} 1 & 0 \\ 0 & \tan^2\gamma \end{bmatrix} \mathbf{U}^H(\psi,\tau,\nu) \tag{3}$$

where $\quad a > 0, \quad \mathbf{U}(\psi,\tau,\nu) = e^{\psi\mathbf{J}}e^{\tau\mathbf{K}}e^{\nu\mathbf{L}} \quad$ is unitary,

$$e^{\psi\mathbf{J}} = \cos\psi\mathbf{I} + \sin\psi\mathbf{J} \quad e^{\tau\mathbf{K}} = \cos\tau\mathbf{I} + \sin\tau\mathbf{K} \quad e^{\nu\mathbf{L}} = \cos\nu\mathbf{I} + \sin\nu\mathbf{L}$$

and $\quad \mathbf{I} = \begin{bmatrix} 1 & 0 \\ 0 & 1 \end{bmatrix}, \quad \mathbf{J} = \begin{bmatrix} 0 & -1 \\ 1 & 0 \end{bmatrix}, \quad \mathbf{K} = \begin{bmatrix} 0 & i \\ i & 0 \end{bmatrix}, \quad \mathbf{L} = \begin{bmatrix} -i & 0 \\ 0 & i \end{bmatrix}.$

We now discuss the physical significance of each of the parameters in the Huynen decomposition. The descriptor a, called the radar scatterer magnitude, gives a measure of scatterer size and is the larger eigenvalue of $\mathbf{S}$. The angles $\psi \in [0,\pi]$ and $\tau \in [-45°, 45°]$ are the tilt angle and ellipticity, respectively, of the polarization state that leads to maximum power received from the scatterer. This definition agrees with intuition for simple scatterers, for example, a vertical dipole has $\psi = 90°$. The angle ν is the scatterer skip angle and is related to the number of bounces of the reflected signal, $-45° \leq \nu \leq 45°$. Odd-bounce mechanisms correspond to $\nu = 0°$ whereas even-bounce mechanisms correspond to $\nu = \pm 45°$. The angle γ which satisfies $0° \leq \gamma \leq 45°$ is called the characteristic angle of the scatterer and it gives the ratio of the maximum and minimum eigenvalues of the scattering matrix. The last descriptor needed to fully define the scattering matrix is the absolute phase ρ of the target. Huynen states that the absolute phase is a mixed target parameter which depends on the distance from the radar to the target. In some cases, modern radars, if properly calibrated, may be able to recover the range-independent absolute phase of the scattering matrix (defined as the phase shift between horizontally polarized incident and reflected electric fields evaluated at the scattering center location). If so, the absolute phase ρ would characterize the material composition of the scattering center. Examples of canonical scattering center types that we wish to detect are pictured in Figure 1 along with their associated scattering matrices and Huynen parameters.

Let $\mathbf{S}_n$ be the *nominal* scattering matrix corresponding to a particular type of scattering center (*i.e.* dipole, dihedral, etc.); the nominal scattering matrix is associated with a scattering center that has amplitude $a = 1$, phase $\rho = 0$ and tilt $\psi = 0$. Then from (3), we see that a general scattering center whose type is the same as that of the nominal scatterer may be written as

$$\mathbf{S} = ae^{j\rho}(e^{\psi\mathbf{J}})^*\mathbf{S}_n(e^{\psi\mathbf{J}})^H \tag{4}$$

Let $\vec{T}_{cn}$ and $\vec{T}_{rn}$ be the nominal target scattering vectors corresponding to $\mathbf{S}_n$. We note from (4) that the elements of $\mathbf{S}$ are linear combinations of the elements of $\mathbf{S}_n$. Hence, we may express the relationship between nominal and general scattering vectors as

$$\vec{T}_c(\vec{\Theta}) = m\mathbf{R}_c(\rho)\mathbf{P}_c(\psi)\vec{T}_{cn} \tag{5}$$
$$\vec{T}_r(\vec{\Theta}) = m\mathbf{R}_r(\rho)\mathbf{P}_r(\psi)\vec{T}_{rn} \quad \text{where}$$
$$\vec{\Theta} = [\, m \quad \rho \quad \psi \,]^T \tag{6}$$

where $\mathbf{R}_c(\rho)$ and $\mathbf{P}_c(\psi)$ are the linear transforms that when applied to $\vec{T}_{cn}$ implement a phase shift by ρ and a tilt by ψ. A similar statement may be made for $\mathbf{R}_r(\rho)$ and $\mathbf{P}_r(\psi)$. The parameterized target model $\vec{T}_c(\vec{\Theta})$ of (5) is the same as that introduced in (2).

We now find expressions for the linear transforms m, $\mathbf{R}_c(\rho)$, $\mathbf{R}_r(\rho)$, $\mathbf{P}_c(\psi)$, and $\mathbf{P}_r(\psi)$. The amplitude shift is simply implemented by the scalar multiply by m. We shall define $\vec{T}_{cn}$ and $\vec{T}_{rn}$ to have unit Euclidean norm, in contrast to $\mathbf{S}_n$ which was taken to have unit matrix norm. Hence, the m of (5) is not, in general, the same as the a of (3), although they serve the same purpose.
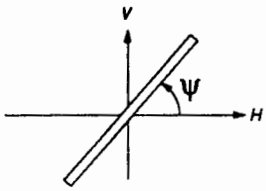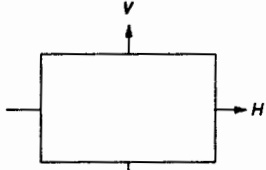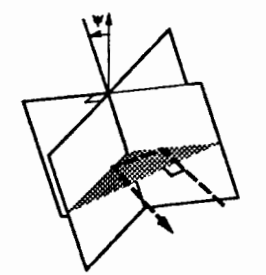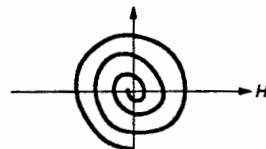
Target Type	Target Geometry	Scattering Matrix (HV basis)	Descriptors (degrees)			
			γ	ν	τ	ψ
Dipole		$\begin{bmatrix} \cos^2\psi & \sin\psi\cos\psi \\ \sin\psi\cos\psi & \sin^2\psi \end{bmatrix}$	0	a	0	ψ
Flat Plate at Normal Incidence or Large Sphere or Trihedral		$\begin{bmatrix} 1 & 0 \\ 0 & 1 \end{bmatrix}$	45	0	0	a
Dihedral or Tophat		$\begin{bmatrix} \cos2\psi & \sin2\psi \\ \sin2\psi & -\cos2\psi \end{bmatrix}$	45	45	0	ψ
Left–Screw Helix		$\frac{1}{2}\begin{bmatrix} 1 & j \\ j & -1 \end{bmatrix}$	0	-45	a	

a—arbitrary

Figure 1: List of canonical scattering centers with geometries, scattering matrices, and Huynen parameters.

It is easy to see from (4) that the phase shift operators are given by

$$\mathbf{R}_c(\rho) = e^{j\rho}$$
$$\mathbf{R}_r(\rho) = \cos\rho\,\mathbf{I} + \sin\rho\,\mathbf{R} \quad \text{where}$$

$$\mathbf{R} \triangleq \begin{bmatrix} 0 & -1 & 0 & 0 & 0 & 0 \\ 1 & 0 & 0 & 0 & 0 & 0 \\ 0 & 0 & 0 & -1 & 0 & 0 \\ 0 & 0 & 1 & 0 & 0 & 0 \\ 0 & 0 & 0 & 0 & 0 & -1 \\ 0 & 0 & 0 & 0 & 1 & 0 \end{bmatrix}$$

and $\mathbf{I}$ is the 6×6 identity.

By expanding (4) using the definitions of $e^{\psi\mathbf{J}}$ and of $\mathbf{J}$ we find that the tilt transforms for the complex and real scattering vectors are

$$\mathbf{P}_c(\psi) = \cos^2\psi\,\mathbf{I} + \sin\psi\cos\psi\,\mathbf{P}_{c1} + \sin^2\psi\,\mathbf{P}_{c2}$$

$$\text{where} \quad \mathbf{P}_{c1} \triangleq \sqrt{2}\begin{bmatrix} 0 & -1 & 0 \\ 1 & 0 & -1 \\ 0 & 1 & 0 \end{bmatrix} \quad \mathbf{P}_{c2} \triangleq \begin{bmatrix} 0 & 0 & 1 \\ 0 & -1 & 0 \\ 1 & 0 & 0 \end{bmatrix}$$

and

$$\mathbf{P}_r(\psi) = \cos^2\psi\mathbf{I} + \sin\psi\cos\psi\mathbf{P}_{r1} + \sin^2\psi\mathbf{P}_{r2}$$

$$\text{where} \quad \mathbf{P}_{r1} \triangleq \sqrt{2}\begin{bmatrix} 0 & 0 & -1 & 0 & 0 & 0 \\ 0 & 0 & 0 & -1 & 0 & 0 \\ 1 & 0 & 0 & 0 & -1 & 0 \\ 0 & 1 & 0 & 0 & 0 & -1 \\ 0 & 0 & 1 & 0 & 0 & 0 \\ 0 & 0 & 0 & 1 & 0 & 0 \end{bmatrix} \quad \mathbf{P}_{r2} \triangleq \begin{bmatrix} 0 & 0 & 0 & 0 & 1 & 0 \\ 0 & 0 & 0 & 0 & 0 & 1 \\ 0 & 0 & -1 & 0 & 0 & 0 \\ 0 & 0 & 0 & -1 & 0 & 0 \\ 1 & 0 & 0 & 0 & 0 & 0 \\ 0 & 1 & 0 & 0 & 0 & 0 \end{bmatrix}$$

2.2 Clutter Model

Based on the discussion in the introduction, we choose to model the clutter scattering vectors $\vec{C}_c$ and $\vec{C}_r$ as either multivariate Gaussian or K-distributed. We do not model correlation between pixels since we are considering only single-pixel-based detectors. The Gaussian distribution is fully-specified by the mean $E[\vec{C}_c]$ and covariance $cov(\vec{C}_c)$. The K-distribution is fully-specified by the shape parameter α, in addition to the mean and covariance [8].

In order to compare the models to the distributions of real terrain clutter we have performed a statistical analysis [14] of real forest clutter measured by a testbed rail-SAR operated by The ElectroScience Laboratory of The Ohio State University [15,16]. The SAR operates over the frequency range (0.2-1.6 GHz) and has a resolution of approximately 1 ft $\times$ 1.5 ft. We estimated the mean and covariance of the forest clutter using the standard unbiased estimates. The experimental results presented in polar format with angles in degrees are

$$E[\vec{C}_c] = 10^{-5}[\ 0.2533\angle130.9 \quad 0.0114\angle-166.8 \quad 0.2960\angle-137.7\ ]^T \tag{7}$$

$$cov(\vec{C}_c) = \Sigma_c = 10^{-7}\begin{bmatrix} 0.2347\angle0 & 0.0107\angle121.3 & 0.0366\angle-110.3 \\ \cdot & 0.0608\angle0 & 0.0117\angle-159.0 \\ \cdot & \cdot & 0.1275\angle0 \end{bmatrix} \tag{8}$$

$$E[\vec{C}_r] = 10^{-5}[\ -0.166 \quad 0.191 \quad -0.011 \quad -0.003 \quad -0.219 \quad -0.199\ ]^T \tag{9}$$

$$cov(\vec{C}_r) = \Sigma_r = 10^{-7}\begin{bmatrix} 0.1135 & 0.0040 & -0.0031 & -0.0046 & -0.0060 & 0.0147 \\ \cdot & 0.1212 & 0.0045 & -0.0025 & -0.0196 & -0.0067 \\ \cdot & \cdot & 0.0307 & -0.0003 & -0.0061 & 0.0019 \\ \cdot & \cdot & \cdot & 0.0301 & -0.0023 & -0.0049 \\ \cdot & \cdot & \cdot & \cdot & 0.0633 & -0.0010 \\ \cdot & \cdot & \cdot & \cdot & \cdot & 0.0642 \end{bmatrix} \tag{10}$$

where the complex and real covariance matrices are complex conjugate symmetric and symmetric, respectively, and hence are fully specified by their upper triangular portions. Notice from (7)–(10) that the pixel values are essentially zero mean and that, for any polarization, the real and imaginary parts of a pixel value are essentially uncorrelated and have equal variance. These observations agree with other findings [8] and suggest that a circular complex random variable representation may be used to model the clutter [3,17]. In Section 4, we simulate forest clutter using the Gaussian and K-distribution with zero mean and with the covariance given by (8). Using the technique of [8] we estimate the shape parameter of the K-distribution to be $\alpha = 0.757$.

3. Polarimetric GLRT

In this section, we present the GLRT decision statistics and their distributions assuming Gaussian clutter and varying partial knowledge of the parameter vector $\vec{\Theta}$ of (6) and (2). We relate these polarimetric GLRTs to existing detectors such as the standard LRT, the OPD, and the PWF. We present the decision statistic for a PGLRT detector that assumes unknown target amplitude m, phase ρ, and orientation angle ψ. Given that a particular scattering

center type is to be detected in a SAR image, these three degrees of freedom (m, ρ, ψ) of the six that are available in the symmetric scattering matrix are unknown in many applications.

We have found that the ML estimates of m and ρ for K-distributed clutter are the same as those for Gaussian clutter, hence the decision statitics for K-distributed clutter for unknown m and ρ are available in closed form. However, the distributions of these decision statistics for K-distributed clutter are not available. Finally, a closed form expression for the ML estimate of tilt angle ψ is not available for Gaussian nor K-distributed clutter, hence, the decision statistic for unknown ψ involves a bounded one-dimensional search. These results are fully discussed in [14].

For the rest of this section, we assume that the clutter component is Gaussian distributed with zero mean and known covariance Σ. We will use the real 6-vector representation of (1), however, we will drop the subscript $_r$ notation for simplicity. In Section 4, we simulate the performance of the PGLRT designed for K-distributed clutter. Analytical performance results are not available for the K-distributed clutter scenario.

3.1 PLRT for completely known target (= matched filter)

First, we consider the case of detecting a completely known target in correlated Gaussian clutter. As we shall see, this is the classical test for Gaussian hypotheses with uncommon means and common covariances [18].

Let $\vec{X}_w$ be the whitened measurement vector

$$\vec{X}_w \triangleq \Sigma^{-1/2}\vec{X}.$$

where Σ is the clutter covariance matrix. The hypothesis test for the whitened measurement is described by

$$
\begin{aligned}
H_0: \quad & \vec{X}_w = \vec{W} \\
H_1: \quad & \vec{X}_w = \vec{W} + m\mathbf{R}(\rho)\Sigma^{-1/2}\mathbf{P}(\psi)\vec{T}_n = \vec{W} + m\mathbf{R}(\rho)\vec{K}_w = \vec{W} + m\vec{U}.
\end{aligned}
\tag{11}
$$

where $\vec{W}$ is the white clutter component with $cov(\vec{W}) = I$, $\vec{K}_w \triangleq \Sigma^{-1/2}\mathbf{P}(\psi)\vec{T}_n$, and $\vec{U} \triangleq \mathbf{R}(\rho)\vec{K}_w$. Equation (11) follows from the assumption that $\Sigma^{-1/2}$ and $\mathbf{R}(\rho)$ commute. This assumption holds since the clutter may be represented as a complex circular random variable as supported by our findings in Section 2.2.

The distribution of the whitened measurement is

$$
\begin{aligned}
\vec{X}_w: \quad & N(\ hm\vec{U},\ \mathbf{I}\ ) \quad \text{where} \\
H_0: \quad & h = 0 \quad\quad\quad \text{(target absent)} \\
H_1: \quad & h = 1 \quad\quad\quad \text{(target present)}.
\end{aligned}
$$

The log likelihood ratio is

$$
\begin{aligned}
\ln\Lambda(\vec{X}_w) \quad &\triangleq\quad \ln\frac{p_1(\vec{X}_w)}{p_0(\vec{X}_w)} \\
&=\quad \ln\frac{q\exp[-\frac{1}{2}(\vec{X}_w - m\vec{U})^T\mathbf{I}(\vec{X}_w - m\vec{U})]}{q\exp[-\frac{1}{2}\vec{X}_w^T\mathbf{I}\vec{X}_w]} \\
&=\quad m\vec{U}^T\vec{X}_w - \frac{1}{2}m^2\vec{U}^T\vec{U}
\end{aligned}
\tag{12}
$$

From here we see that a sufficient statistic for this detection problem is $\vec{U}^T\vec{X}_w$ which we scale by $1/\sqrt{\vec{K}_w^T\vec{K}_w}$ to normalize the variance. The resulting Gaussian decision statistic is

$$\vec{S}(\vec{X}_w) = \vec{U}^T\vec{X}_w/\sqrt{\vec{K}_w^T\vec{K}_w}$$

Although a closed form solution for the ML estimate of ψ is not available for a general scattering center, we can report results for some particular scattering center types. The flat plate, trihedral, and sphere are polarimetrically symmetric with respect to rotation about the line of sight (*i.e.* their scattering matrix is not a function of ψ, or ψ is not well defined for these scattering centers). Hence $\vec{S}(\psi)$ of (14) is a constant function of tilt angle ψ and there is no need to carry out the maximization. The GLRT detector for these targets assuming unknown amplitude, phase, and tilt angle are the same as that found in Section 3.2 . The same findings hold for the right or left screw helix since the act of tilting a helix is indistinguishable from an absolute phase shift.

3.4 PGLRT for completely unknown target (= PWF)

Suppose that the target component $\vec{T}$ of the measurement $\vec{X}$ is completely unknown. The likelihood function for Gaussian clutter is

$$f(\vec{T}) = q \exp[-\frac{1}{2}(\vec{X} - \vec{T})^T \Sigma^{-1}(\vec{X} - \vec{T})]$$

which is maximized by simply choosing $\vec{T} = \vec{X}$. The resulting PGLRT is the standard log likelihood function with the unknown target component replaced by $\vec{T}_{ML} = \vec{X}$

$$
\begin{aligned}
2\ln \Lambda(\vec{X}) &= 2\ln \frac{q \exp[-\frac{1}{2}(\vec{X} - \vec{X})^T \Sigma^{-1}(\vec{X} - \vec{X})]}{q \exp[-\frac{1}{2}\vec{X}^T \Sigma^{-1}\vec{X}]} \\
&= \vec{X}^T \Sigma^{-1}\vec{X}.
\end{aligned}
$$

This is just the polarization whitening filter (PWF) [1,2,3]. Hence, another interpretation of the PWF is that of being the PGLRT for a completely unknown target.

4. THEORETICAL AND SIMULATED PERFORMANCE CURVES

4.1 Gaussian clutter

This section investigates the performance of the PGLRTG(ρ, m, ψ), the PGLRT designed for Gaussian clutter that assumes unknown target phase ρ, amplitude m, and tilt ψ. In Section 3.3 we argued that the performance of the PGLRTG(ρ, m, ψ) for the flat plate, trihedral, sphere, and helix is the same as that of the OPD=PGLRTG(ρ, m) due to the symmetry of these scattering centers with respect to tilt ψ. Hence, in this section we restrict ourselves to the detection of dipoles and dihedrals.

Closed form expressions for the ML estimates of ψ for the dipole and dihedral are unavailable. Hence, in Section 3.3 we were unable to develop expressions for the theoretical performance of the PGLRTG(ρ, m, ψ) when applied to dipoles and dihedrals. In order to characterize the performance we rely on simulation. The simulations are implemented for Gaussian clutter by computing $\vec{S}(\psi)$ of (14) in increments of $\Delta\psi = 5°$ and choosing the maximum. A similar approach is used for K-distributed clutter except that the likelihood function is more complex in that case.

We compare the simulated performance of the PGLRTG(ρ, m, ψ) with the theoretical performance of the OPD and PWF. Since the performance of the PGLRTG(ρ, m) is identical to that of the OPD we know that the performance of the PGLRTG(ρ, m, ψ) must not exceed that of the OPD. We expect, however, that the PGLRTG(ρ, m, ψ) performs at least as well as the PWF since the PGLRTG(ρ, m, ψ) assumes that three of the six degrees of freedom in a scattering center response are known whereas the PWF is equivalent to the PGLRTG for a completely unknown target.

In order to describe the signal-to-noise ratio we use two measures:

$$SNR_1 \quad \triangleq \quad \frac{\|m\mathbf{R}(\rho)\mathbf{P}(\psi)\vec{T}\|^2}{\|\Sigma\|} = \frac{m^2}{\|\Sigma\|} \tag{15}$$

$$
\begin{aligned}
SNR_2 &\triangleq [m\mathbf{R}(\rho)\mathbf{P}(\psi)\vec{T}]^T \mathbf{\Sigma}^{-1}[m\mathbf{R}(\rho)\mathbf{P}(\psi)\vec{T}] \\
&= [m\mathbf{P}(\psi)\vec{T}]^T \mathbf{\Sigma}^{-1}[m\mathbf{P}(\psi)\vec{T}] = m^2 \vec{K}_w^T \vec{K}_w . \qquad (16)
\end{aligned}
$$

$$
\text{where} \quad \vec{K}_w \triangleq \mathbf{\Sigma}^{-1/2}\mathbf{P}(\psi)\vec{T}
$$

Equation (15) follows from the orthogonality of $\mathbf{R}(\rho)$ and $\mathbf{P}(\psi)$ and $\|T\| \triangleq 1$. Equation (16) follows from the definition of $\vec{K}_w$, $\mathbf{\Sigma}^{-1}\mathbf{R}(\rho) = \mathbf{R}(\rho)\mathbf{\Sigma}^{-1}$, and $\mathbf{R}(\rho)^T \mathbf{R}(\rho) = \mathbf{I}$.

SNR_1 is useful for describing the strength of the target component relative to the largest eigenvalue of $\mathbf{\Sigma}$. This SNR measure is not sensitive to the relative locations of the target component and clutter distribution in polarization space and hence, it is independent of the target tilt angle ψ. It is a good measure for understanding the degree to which the tilt angle of a canonical scattering center can affect its ability to be detected in clutter that is correlated across polarization.

SNR_2, sometimes called the "generalized SNR", is a more meaningful measure for quantifying the degree to which the target component is located in a high-clutter-density region of polarization space. SNR_2 varies with target tilt angle ψ. Its value dictates whether a target at one tilt angle is more easily detected than the same target with a different tilt angle.

Figure 2 shows ROC curves comparing the $PGLRTG(\rho, m, \psi)$, OPD, and PWF for $SNR_1 = 8$dB. Theoretical curves are used to display the OPD and PWF performance and simulated curves are used for the $PGLRTG(\rho, m, \psi)$. Plots (a) and (b) are for a dipole and dihedral, respectively. Each of the plots show curves for $\psi = 0°$ and $60°$.

(a) dipole   (b) dihedral

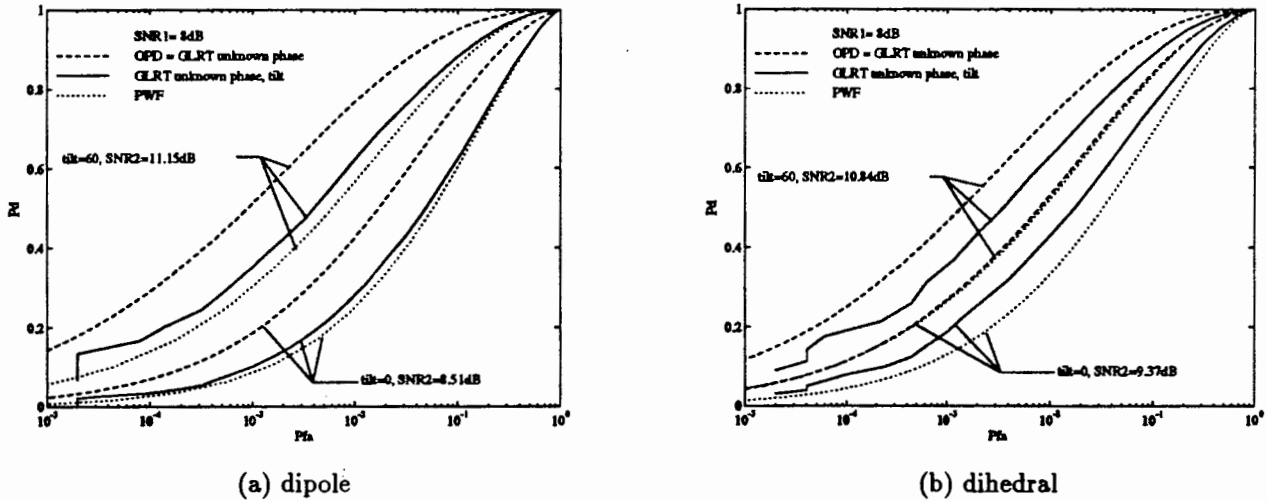Figure 2: Simulated ROC curves for $PGLRTG(\rho, m, \psi)$ compared with theoretical OPD and PWF ROC curves. The plots are for (a) dipoles and (b) dihedrals with $\psi = 0°$ and $60°$. $SNR_1 = 8dB$ and 50,000 trials.

In Figure 2(a) we see that the $PGLRTG(\rho, m, \psi)$ performs better than the PWF over the entire range of P_F when detecting a dipole. The improvement in P_D is approximately 1-2% and 5% for a dipole at $\psi = 0°$ and $60°$, respectively over a wide range of P_F. For the dihedral of (b), the $PGLRTG(\rho, m, \psi)$ increases its improvement over the PWF. For example, for $P_F = 10^{-3}$, the $PGLRTG(\rho, m, \psi)$ has approximately a 6.5% and 9% higher probability of detection for $\psi = 0°$ and $60°$, respectively. The $PGLRTG(\rho, m, \psi)$ does not perform as well as the OPD = $PGLRTG(\rho, m)$ which assumes more target knowledge. The figure shows that ignorance of the target tilt angle can cause a loss of up to 18% in the probability of detection for a given probability of false alarm.

Next we compare the $PGLRTG(\rho, m, \psi)$ with the OPD and PWF by plotting P_F versus SNR_1 for fixed $P_D = 0.8$.

Figure 3 shows such plots for (a) dipoles and (b) dihedrals at tilt angles of $\psi = 0^o$ and 60°. The OPD and PWF curves are theoretical and the PGLRTG(ρ, m, ψ) curves for the dipole and dihedral are based on 20,000 and 50,000 simulations, respectively. Some of the theoretical curves do not extend to $SNR_1 = 12$ dB due to numerical difficulty involved with inverting the noncentral χ^2 distribution to set the threshold and then integrating under the tail of the central χ^2 distribution to compute P_F.

In Figure 3 we see that the PGLRTG(ρ, m, ψ) provides a lower probability of false alarm than the PWF over the entire range of SNR_1 values. This improvement is more pronounced for the dihedral and for higher SNR_1. For example, for $SNR_1 = 9dB$ and $\psi = 60^o$, P_F[PWF]=1.67P_F[PGLRTG(ρ, m, ψ)] for the dipole and P_F[PWF]=2.16P_F[PGLRTG(ρ, m, ψ)] for the dihedral. As expected, the PGLRTG(ρ, m, ψ) does not perform as well as the OPD which assumes that ψ is known. Recall that the performance of the PGLRTG(ρ, m, ψ) applied to the flat plate, sphere, trihedral, and helical scattering centers is equal to that of the OPD since their responses are independent of tilt angle, except for a phase shift in the case of the helix.
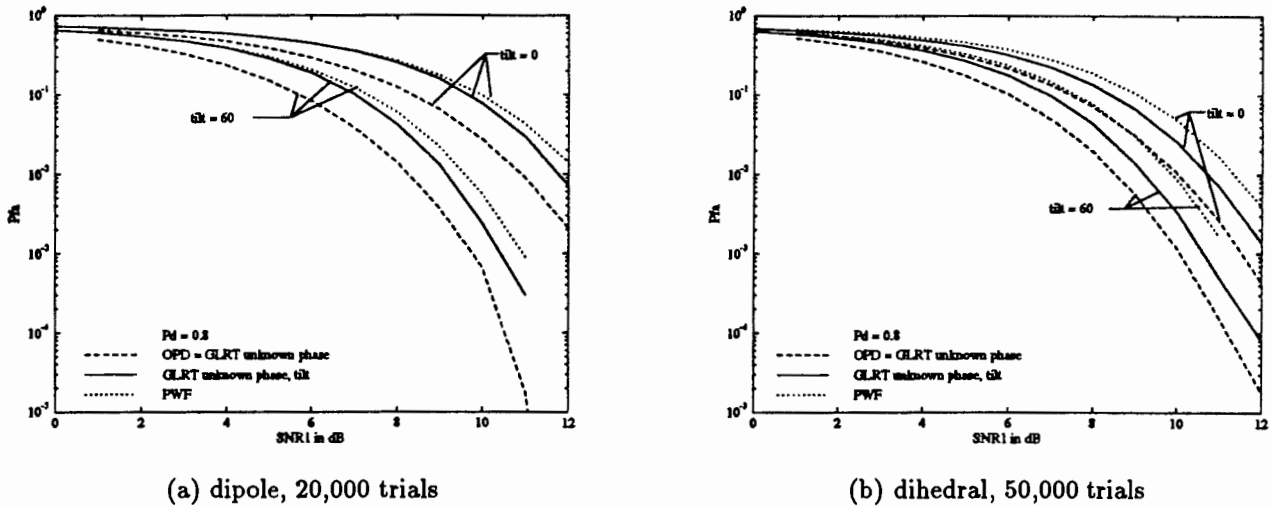

(a) dipole, 20,000 trials

(b) dihedral, 50,000 trials

Figure 3: Comparison of PGLRTG(ρ, m, ψ) with OPD and PWF using plots of P_F vs SNR_1 for fixed $P_D = 0.8$. The PGLRTG(ρ, m, ψ) curves are simulated and the OPD and PWF curves are theoretical.

4.2 K-distributed clutter

In this section we assess the performance of detectors designed for Gaussian clutter and applied to K-distributed clutter scenarios. If acceptable performance is achieved using Gaussian detectors then they may be chosen due to their computational advantage over the K-distributed detectors.

We consider a horizontal dihedral with $SNR_1 = 4dB$. The clutter is K-distributed with parameter $\alpha = 1.51$. Figure 4 shows simulated ROC curves for various detectors that we have discussed; some of which assume K-distributed clutter (the solid curves in the figure) and others which assume Gaussian clutter. For $P_F = 10^{-3}$, we see that P_D for the PLRTK exceeds that of the PLRTG by a factor of 5.5. Similarly, the PGLRTK(m, ρ) performance exceeds that of the OPD=PGLRTG(m, ρ) by a factor of 4.75 and the PGLRTK(m, ρ, ψ) performance exceeds the PWF performance by a factor of approximately 2. It is interesting to note, for example, that the K-clutter-based detector that assumes unknown tilt angle performs as well as the Gaussian clutter-based detector that assumes the tilt angle is known.

We conclude that the statistical mismatch associated with applying Gaussian based detectors in K-distributed clutter applications can cause objectionable performance degradation in low SNR cases with shape parameters of

at least $\alpha = 1.5$ and below. A judgement may be made as to whether the additional performance capability of the K-distributed-clutter based detectors justify their greater computational expense.
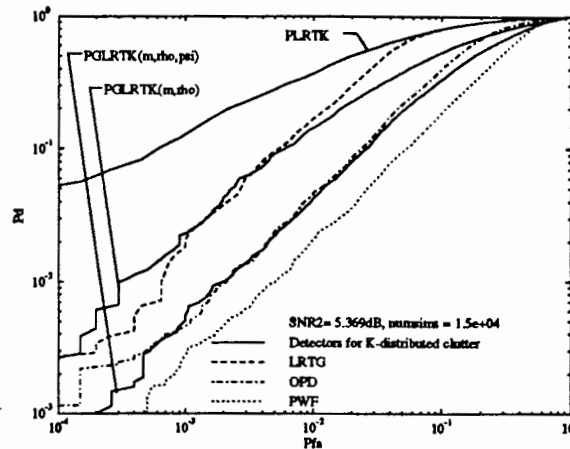

Figure 4: Simulated ROC curves for various detectors applied to the problem of detecting a horizontal dihedral in K-distributed clutter with $\alpha = 1.51$. $SNR_1 = 4dB$ and 15,000 trials.

5. CONCLUSIONS

We have described a family of polarimetric generalized likelihood ratio tests (PGLRTs) for single-pixel-based detection. The detectors are based on a deterministic model of the polarimetric response of a target scattering center. The model is parameterized by the scattering center amplitude, phase, and orientation angle about the line of sight. The family of detectors is generated my making different assumptions about which of the model parameters are known. We have related this family of detectors to existing polarimetric detectors such as the optimal polarimetric detector (OPD) and the polarization whitening filter (PWF). The OPD is found to be equivalent to the PGLRT that assumes unknown target amplitude and phase under certain assumptions. The PWF has the interpretation of the PGLRT that assumes the scattering center response is completely unknown.

We have introduced a new polarimetric detector designed to detect a certain type of scattering center (dipole, dihedral, etc.) regardless of its amplitude, phase, and orientation angle about the radar line of sight. The performance of this detector lies between that of the OPD and the PWF.

Finally, we have considered performance of polarimetric detectors in Gaussian and K-distributed clutter. We have noted an objectionable loss in performance in the statistical mismatch case of applying Gaussian detectors in K-distributed clutter scenarios relative to the performance of detectors designed for K-distributed clutter.

6. ACKNOWLEDGMENTS

7. REFERENCES

1. L. M. Novak, M. B. Sechtin, and M. J. Cardullo, "Studies of target detection algorithms that use polarimetric radar data," *IEEE Transactions on Aerospace and Electronic Systems*, vol. AES-25, pp. 150–165, March 1989.

2. L. M. Novak and M. C. Burl, "Optimal speckle reduction in polarimetric SAR imagery," *IEEE Transactions on Aerospace and Electronic Systems*, vol. AES–26, pp. 293–305, March 1990.

3. L. M. Novak, M. C. Burl, R. D. Chaney, and G. J. Owirka, "Optimal processing of polarimetrc synthetic-aperture radar imagery," *The Lincoln Laboratory Journal*, vol. 3, pp. 273–290, Summer 1990.

4. W. W. Irving, G. J. Owirka, and L. M.Novak, "Adaptive processing of polarimetric sar imagery," in *24th Asilomar Conference on Signals, Systems, and Computers*, (Pacific Grove, CA), pp. 388–398, November 1990.

5. L. M. Novak and M. B. Sechtin, "Target detection algorithms that use polarimetric radar data: New results," in *Proceedings of the Polarimetric Technology Workshop*, vol. I.1, (Redstone Arsenal, Alabama), pp. 537–555, August 16–18 1988.

6. H. Lim, A. A. Swartz, H. A. Yueh, J. A. Kong, R. T. Shin, and J. J. van Zyl, "Classification of earth terrain using synthetic aperture radar images," *J. Geophys. Res.*, vol. 93, pp. 15252–15260, December 1988.

7. H. A. Yueh, A. A. Swartz, J. A. Kong, R. T. Shin, and L. M. Novak, "Bayes classification of terrain cover using normalized polarimetric data," *J. Geophys. Res.*, vol. 93, pp. 15261–15267, December 1988.

8. S. H. Yueh, J. A. Kong, J. K. Jao, R. T. Shin, H. A. Zebker, T. L. Toan, and H. Ottl, "Chapter 4: K-distribution and polarimetric terrain radar clutter," in *PIER-3: Progress in Electromagnetics Research: Polarimetric Remote Sensing* (J. A. Kong, ed.), New York: Elsevier, 1990.

9. D. C. Schleher, ed., *Automatic Detection and Radar Data Processing*, ch. Detection in Non-Gaussian Clutter. Dedham, MA: Artech House, Inc., 1980.

10. E. Jakeman, "On the statistics of K-distributed noise," *J. Phys. A: Math. Gen.*, vol. 13, pp. 31–48, 1980.

11. J. K. Jao, "Amplitude distribution of composite terrain radar clutter and the K-distribution," *IEEE Transactions on Antennas and Propagation*, vol. AP-32, pp. 1049–1062, October 1984.

12. H. L. V. Trees, *Detection, Estimation, and Modulation Theory: Part I.* New York: Wiley, 1968.

13. J. R. Huynen, *Phenomenological Theory of Radar Targets.* PhD thesis, Technical University, Delft, The Netherlands, 1970.

14. R. L. Dilsavor, *Detection of Target Scattering Centers in Terrain Clutter Using an Ultra-Wideband, Fully-Polarimetric Synthetic Aperture Radar.* PhD thesis, The Ohio State University, September 1993. Also: SPANN Laboratory Technical Report TR-93-05.

15. B. L. Chan, "Fourier based radar imaging techniques," Master's thesis, The Ohio State University, August 1993.

16. "Radar comparison program final report," Tech. Rep. AZER-2913, Loral Defense Systems - Arizona, April 1993.

17. M. L. Eaton, *Multivariate Statistics - A Vector Space Approach.* New York: John Wiley and Sons, 1983.

18. L. L. Scharf, *Statistical Signal Processing.* Reading, Massachusetts: Addison-Wesley, 1991.